Applied Catalysis B: Environmental 115–116 (2012) 179–189

Contents lists available at SciVerse ScienceDirect

Applied Catalysis B: Environmental

journal homepage: www.elsevier.com/locate/apcatb

# The effect of synergy between $Cr_2O_3$-$CeO_2$ and USY zeolite on the catalytic performance and durability of chromium and cerium modified USY catalysts for decomposition of chlorinated volatile organic compounds

Qinqin Huang[a,b], Zhonghua Meng[a], Renxian Zhou[a,*]

[a] Institute of Catalysis, Zhejiang University, Hangzhou 310028, PR China
[b] Shanghai Research Institute of Petrochemical Technology, Shanghai 201208, PR China

ARTICLE INFO

*Article history:*
Received 23 June 2011
Received in revised form 8 December 2011
Accepted 16 December 2011
Available online 27 December 2011

*Keyword:*
$Cr_2O_3$-$CeO_2$-USY catalysts
CVOCs decomposition
Deeper oxidation ability
Catalytic performance
Durability

ABSTRACT

The chromium and cerium modified USY zeolite catalysts ($Cr_2O_3$-$CeO_2$-USY) were prepared by impregnation method and investigated in terms of catalytic decomposition of dichloromethane (DCM), trichloroethylene (TCE) and 1,2-dichloroethane (DCE). The results show that there are two types of active sites in the catalysts. The acidic site is the active center for dehydrochlorination of CVOCs, and the metallic xoide is the center providing active oxygen species for CVOCs deeper oxidation. The interaction between $Cr_2O_3$ and $CeO_2$ species optimizes the concentration ratio of strong acid sites to weak acid sites and improves the mobility of oxygen species over $Cr_2O_3$-$CeO_2$-USY catalysts, which is beneficial to the dehydrochlorination and deeper oxidation of chlorinated volatile organic compounds (CVOCs), respectively. $Cr_2O_3$-$CeO_2$-USY catalyst with 17.5 wt.% loading of $Cr_2O_3$ ($17.5Cr_2O_3$-$12.5CeO_2$-USY) presents better catalytic performance for CVOCs decomposition along with higher selectivity to HCl and $CO_2$ formation, which can be due to the higher percentage of strong acidity, more accessible oxygen species, and the stronger synergy between $Cr_2O_3$-$CeO_2$ and USY zeolite. In addition, the stronger interaction between $Cr_2O_3$ and $CeO_2$, along with the synergy between $Cr_2O_3$-$CeO_2$ and USY zeolite over $17.5Cr_2O_3$-$12.5CeO_2$-USY results in less coke deposit, slight HCl attack on the catalysts and improved resistance to chlorination of active components. Therefore, $17.5Cr_2O_3$-$12.5CeO_2$-USY shows the better durability and structure stability during the long term exposure to DCE.



## 1. Introduction

Chlorinated volatile organic compounds (CVOCs), one of the major sources of air pollution, are known to be hazardous to the environment and human health [1]. Among all the technologies for CVOCs elimination, catalytic oxidation is considered as an attractive one for the decomposition of CVOCs due to its high catalytic performance for the destruction of low concentrations of contaminant (<1000 ppm), high selectivity to harmless by-products, and less severe conditions (<500 °C) [2,3].

The catalysts used for catalytic oxidation of CVOCs mainly base on four types, noble metals [4], transition metal oxides [5], rare earth oxides [6,7] and zeolite [8,9] catalysts. Among these catalysts, transition metal oxides catalysts show relatively better performance and resistance to deactivation compared to the other three type catalysts, which are easily poisoned by chlorine or deactivated by coke deposit [10,11].

It is known that active metal species in the catalyst have different abilities to promote the catalytic activity for CVOCs destruction. Each metal will catalyze the reaction through different reaction mechanisms, rendering differences in the distribution of the combustion products and the overall behavior of the process [12–14]. Lots of previous researches [15–19] have reported that chromium based catalysts show high performance for CVOCs catalytic oxidation. It has been reported that $CrO_x/TiO_2$ exhibits higher activity for destruction of CVOCs compared with $CrO_x$ supported on other metal oxides [20–23]. Kang et al. [24,25] have evaluated several carbon supported chromium catalysts and found that oxidative treatment of the support increases its acidity, leading to the improved activity of the carbon-supported chromium oxide catalysts for complete oxidation of DCM. Oliveira et al. have found that pillared montmorillonite with high specific surface is the effective support to disperse catalytic active phase Cr, and the related Cr-impregnated bentonite show high activity for the total oxidation of cholorobenzene [26]. Chromium supported on zeolite catalysts are very active for the decomposition of CVOCs, due to its high adsorption capacity along with the excellent catalytic activity, which makes it suitable for adsorption/catalysis bifunctional

* Corresponding author. Tel.: +86 571 88273290; fax: +86 571 88273283.
*E-mail address:* zhourenxian@zju.edu.cn (R. Zhou).

0926-3373/$ – see front matter. 
doi:10.1016/j.apcatb.2011.12.028

systems for energy-saving treatment of low concentration of CVOCs [27,28]. However, for all the chromium oxide supported catalysts, the migration and/or loss of active sites may be the main factor resulting in deactivation of the catalysts. Moreover, the formation of the extremely toxic chromium oxychloride at low temperature also restricts the application of the catalysts [29,30].

In our previous work, we have found that the addition of $CeO_2$ to USY zeolite enhances the process of DCE dehydrochlorination to form $C_2H_3Cl$, favors the further oxidation of $C_2H_3Cl$ and improves the selectivity to $CO_2$ formation compared with USY zeolite [31–33]. In this paper, we aim to evaluate the effect of the interaction between $Cr_2O_3$ and $CeO_2$ species as well as the synergy between $Cr_2O_3$-$CeO_2$ and USY zeolite on the catalytic activity, the products distribution and the durability of $Cr_2O_3$-$CeO_2$-USY catalysts during the decomposition of DCE, DCM and TCE.

## 2. Experimental

### 2.1. Catalysts preparation

The molar ratio of $SiO_2/Al_2O_3$ for USY zeolite is 5.3. The catalyst signed as 12.5$CeO_2$-USY with $CeO_2$ loading of 12.5 wt.% was prepared by USY zeolite impregnated with $Ce(NO_3)_3{\cdot}6H_2O$ (AR, 98.0%) solution. The catalysts signed as 11.5$Cr_2O_3$-12.5$CeO_2$-USY, 17.5$Cr_2O_3$-12.5$CeO_2$-USY and 23.5$Cr_2O_3$-12.5$CeO_2$-USY were prepared by USY zeolite co-impregnated with $Ce(NO_3)_3{\cdot}6H_2O$ and $Cr(NO_3)_3{\cdot}9H_2O$ solutions. The $Cr_2O_3$ loading is 11.5, 17.5 and 23.5 wt.% of 12.5$CeO_2$-USY catalyst's weight, respectively. All the impregnated catalysts were dried at 100 °C for 2 h, followed by calcination in air at 350 °C for 0.5 h and further at 550 °C for 2 h.

### 2.2. Catalysts characterization

The surface area of the catalysts was determined by $N_2$ adsorption/desorption at liquid nitrogen temperature on a Coulter OMNISORP-100 apparatus. The samples were degassed under vacuum for 3 h at 200 °C before the measurements. Specific surface area was calculated using the Brunauer–Emmett–Teller (BET) equation.

X-ray diffraction (XRD) measurement was performed on an ARL X'TRA X-ray Diffractometer (Thermo Eelctron Corporation, USA), with Cu Kα radiation at 40 kV and 40 mA in a scanning range of 3–70° (2$\theta$). The crystallinity analysis of the catalysts was carried out under the same condition except for the scanning process. The scanning was operated in the range of 3–90° (2$\theta$) with a step size of 0.02° and a step time of 2.5 s.

The X-ray photoelectron spectroscopy (XPS) analysis was recorded with a PHI5000c spectrometer at 1486.6 eV and 12.5 kV using Al Kα radiation. The samples were pressed into thin discs and mounted on a sample rod placed in a pretreatment chamber. All the binding energy (BE) values were calibrated using the C 1s peak at 284.8 eV.

The ammonia temperature-programmed desorption ($NH_3$-TPD) was performed in a quartz fixed-bed micro-reactor equipped with thermal conductivity detector (TCD). Prior to the adsorption of ammonia, the catalyst (100 mg) was pretreated in a $N_2$ stream (99.99%, 35 mL $min^{-1}$) at 500 °C for 0.5 h. After being cooled down to 100 °C, the catalyst was exposed to a flow of 20 vol.% $NH_3/N_2$ mixture (30 mL $min^{-1}$) for 30 min, and then treated in a $N_2$ flow for 1 h in order to remove physically bound ammonia. Finally, the desorption performance was carried out in a $N_2$ flow (99.99%, 40 mL $min^{-1}$) from 100 to 600 °C with a heating rate of 10 °C $min^{-1}$. All the profiles were simulated by Gaussian functions, and the quantification of the acid sites was calculated from the area of deconvolution peaks.

The hydrogen temperature-programmed reduction ($H_2$-TPR) was performed in a quartz fixed-bed micro-reactor equipped with TCD, using a 5 vol.% $H_2$/Ar mixture. The catalyst (50 mg) was pretreated in air at 300 °C for 0.5 h. After being cooled down to 100 °C, the reduction was carried out from 100 to 800 °C at a heating rate of 10 °C $min^{-1}$.

The coke content of the catalysts after long term reaction was measured in a Thermogravimetric Analyzer (TGA, PerkinElmer Inc. USA). After being pretreated in a $N_2$ flow (99.99%, 30 mL $min^{-1}$) at 120 °C for 0.5 h, the catalyst was further heated up to 800 °C at a heating rate of 10 °C $min^{-1}$ in a mixture flow (60 mL $min^{-1}$) of 40 vol.% $O_2/N_2$.

The actual content of chromium in the catalysts was measured by inductively coupled plasma atomic emission spectrometry (ICP-AES) on an IRIS Intrepid II XSP (Thermo Eelctron Corporation, USA). The pretreatment of the samples were carried out by full-acid-digestion ($HCl + HNO_3 + HF + HClO_4$) method.

### 2.3. Catalytic activity tests

The catalytic activity tests were carried out in a fixed-bed micro-reactor (quartz glass, 6 mm i.d., 30 cm length) at atmospheric pressure. About 0.20–0.24 g catalyst (40–60 mesh) was placed in the middle of the reactor and the gas hourly space velocity (GHSV) was 15,000 $h^{-1}$ with a total flow of 75 mL $min^{-1}$. The feed gas (DCE, DCM or TCE) was prepared by delivering the liquid by a syringe pump into dry air (dried by silica gel and 5A zeolite), and the concentration of the feed gas was about 1000 ppm with air as balance. The gas stream was analyzed by an on-line gas chromatograph equipped with a packed column (OV 101) and flame ionization detector (FID). Mass spectrum was used for the determination of those detected intermediates ($CH_3Cl$, $C_2H_3Cl$, $CH_3CHO$, $CH_3COOH$ and $C_2Cl_4$). The conversion was calculated using the peak area of DCE, DCM and TCE. The amount of $CH_3Cl$, $C_2H_3Cl$, $CH_3CHO$, $CH_3COOH$ and $C_2Cl_4$ was calculated from the calibration curve of those compounds, respectively. CO was analyzed by an on-line gas chromatograph equipped with a carbon molecular sieve (TDX-01) column and analyzed by FID. CO was first converted to methane by a methanation reactor.

The temperature-programmed surface reaction (TPSR) measurement was carried out under the same condition as catalytic activity. The adsorption of DCE on the catalyst was first carried out at 50 °C. After the adsorption–desorption equilibrium was reached, the catalyst was heated from 50 to 500 °C at a rate of 5 °C $min^{-1}$. The reactant (DCE) and the products (HCl, $Cl_2$ and $CO_2$) were analyzed on-line over a mass spectrometer apparatus (HIDEN QIC-20).

### 2.4. Durability tests

The durability tests for USY, 12.5$CeO_2$-USY and 17.5$Cr_2O_3$-12.5$CeO_2$-USY were performed under the following conditions: the catalyst was exposed to CVOCs stream ([DCE, DCM and TCE] = ~1000 ppm) at given temperatures for 100 h and the total flow was 75 mL $min^{-1}$ with GHSV = 15,000 $h^{-1}$.

## 3. Results and discussion

### 3.1. Characterization results

#### 3.1.1. Texture and structure

Fig. 1 shows the XRD patterns of USY zeolite and modified USY zeolite catalysts. Distinct diffraction peaks ascribed to the framework of USY zeolite are observed over all the catalysts, demonstrating that the framework of USY zeolite is not destroyed by the modification. The diffraction peaks ascribed to fluorite-type

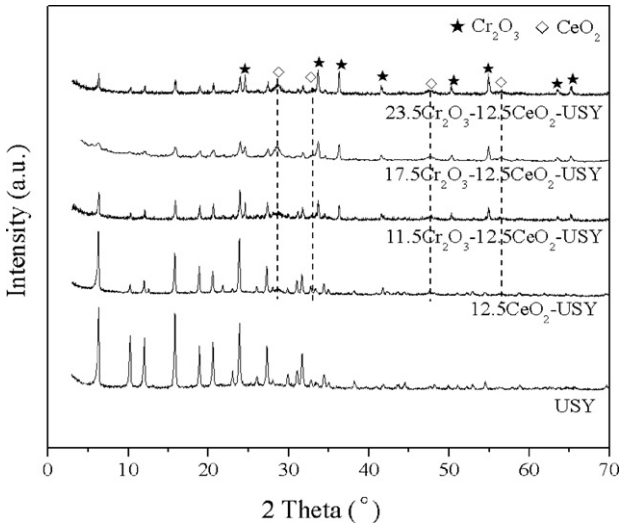


**Fig. 1.** XRD patterns of the catalysts.

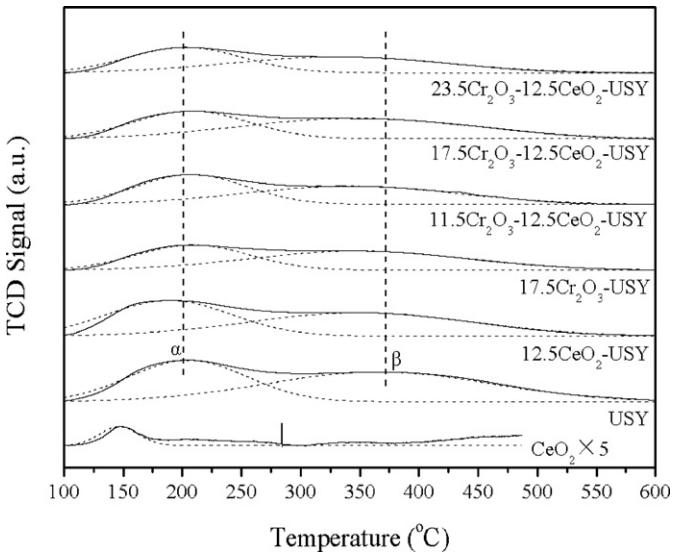


**Fig. 2.** $NH_3$-TPD profiles of the catalysts.

oxide structure of $CeO_2$ are rather weak over 12.5$CeO_2$-USY, indicating the high dispersion of $CeO_2$ species on USY zeolite. However, the signals of $CeO_2$ are obviously detected over $Cr_2O_3$-$CeO_2$-USY catalysts, which become more and more intense as $Cr_2O_3$ content increases. The results may be related to the fact that $Cr^{3+}$ with smaller radius than $Ce^{3+}$ can enter the pore channel of USY zeolite more easily, which hinders the entrance of $Ce^{3+}$ and results in the aggregation of $CeO_2$ particles on USY zeolite. As listed in Table 1, the lattice parameters of $CeO_2$ over $Cr_2O_3$-$CeO_2$-USY catalysts show a reduction compared with that of pure $CeO_2$ (5.4082 Å), which demonstrates that partial $Cr^{3+}$ with smaller radius enters into the crystal lattice of $CeO_2$, causing the shrinkage of the crystal cell. Moreover, some of the chromium element may combine with cerium to form Cr–Ce–O mixed oxide, which is beneficial to enhancing the stability of active components.

The specific surface area of each catalyst is listed in Table 1. It is visible that the surface area of modified USY zeolite catalysts obviously decreases compared with that of USY zeolite. Moreover, the surface area gradually decreases with the increasing $Cr_2O_3$ content. The results suggest that the active species, especially $Cr_2O_3$ species, block the pore channel of USY zeolite, which are consistent with the XRD results.

As the XPS results shown in Table 2, the value of $Ce^{3+}/Ce^{4+}$ increases in 17.5$Cr_2O_3$-12.5$CeO_2$-USY compared with that in 12.5$CeO_2$-USY, indicating that the interaction between $Cr_2O_3$ and $CeO_2$ species favors the formation of $Ce^{3+}$. It has been reported in the literature that the presence of $Ce^{3+}$ is related to the formation of oxygen vacancy [34], which is beneficial to improve the mobility of lattice oxygen, and further enhances the deep oxidation of CVOCs over the catalyst. With respect to the Cr element, the increment of BE value as well as the decrease in the ratio of $Cr^{3+}/Cr^{6+}$ in 17.5$Cr_2O_3$-12.5$CeO_2$-USY suggests that the interaction between $Cr_2O_3$ and $CeO_2$ species promotes the formation of $Cr^{6+}$, which exhibits better oxidation ability, further favoring deep oxidation of CVOCs [35]. In addition, the increase of Ce content in 17.5$Cr_2O_3$-12.5$CeO_2$-USY compared with that in 12.5$CeO_2$-USY also evidences that the co-impregnation of chromium and cerium causes a Ce enrichment in the surface of the catalysts as observed in XRD results.

### 3.1.2. Acidity property

Fig. 2 shows the $NH_3$-TPD profiles of USY zeolite and modified USY zeolite catalysts. Two distinct desorption peaks (peak α and β) are observed over all the catalysts. Peak α is ascribed to weak acid sites, which are associated with the framework Lewis acid sites and aluminum-rich extra framework species [36]. Peak β is assigned to strong acid sites, which are mainly attributed to Brønsted acid sites in the framework of the zeolite [37]. In comparison with USY zeolite, the peak-temperature of peak α shifts to lower temperature over 12.5$CeO_2$-USY, but it slightly moves to higher temperature over 17.5$Cr_2O_3$-USY and $Cr_2O_3$-$CeO_2$-USY catalysts. The results demonstrate that the strength of weak acidity is weakened by $CeO_2$ addition, but is strengthened by addition of $Cr_2O_3$. However, the strength of strong acidity is not affected evidently by either $CeO_2$ or $Cr_2O_3$ species addition according to the little change in peak-temperature of peak β.

The quantitative analysis of acidity distribution is reported in Table 1. Comparing with USY zeolite, the total acidity decreases evidently over modified USY zeolite catalysts, especially over 17.5$Cr_2O_3$-USY and $Cr_2O_3$-$CeO_2$-USY catalysts. The results can be assigned to the covering of acid sites by metal deposits [38] as

**Table 1**
The physical and chemical characteristics of the catalysts.

| Catalysts | Lattice parameters of $CeO_2$ (Å) | $S_{BET}$ ($m^2$/g) | Acidity distribution (mmol $NH_3$/g) | | | | $H_2$ consumption (mmol/g) |
|---|---|---|---|---|---|---|---|
| | | | Total | Weak | Strong | $R_{sw}$[a] | |
| $CeO_2$ | – | – | 0.020 | 0.020 | – | – | 0.49 |
| USY | – | 562.8 | 1.030 | 0.344 | 0.596 | 1.74 | – |
| 12.5$CeO_2$-USY | – | 485.5 | 0.750 | 0.340 | 0.410 | 1.20 | 0.11 |
| 17.5$Cr_2O_3$-USY | – | 294.5 | 0.582 | 0.238 | 0.344 | 1.44 | 0.40 |
| 11.5$Cr_2O_3$-12.5$CeO_2$-USY | – | 403.7 | 0.601 | 0.273 | 0.328 | 1.20 | 0.41 |
| 17.5$Cr_2O_3$-12.5$CeO_2$-USY | 5.4020 | 396.9 | 0.638 | 0.255 | 0.383 | 1.50 | 0.43 |
| 23.5$Cr_2O_3$-12.5$CeO_2$-USY | 5.4031 | 296.2 | 0.506 | 0.232 | 0.274 | 1.18 | 0.44 |

[a] Ratio of strong acidity concentration to weak acidity concentration.

**Table 2**
The coke content, crystallinity, binding energy and relative abundance of main elements for the catalysts.

| Catalyst | Coke content (%) | Crystallinity (%) | Binding energy (eV) | | | Relative abundance (%) | | | | | |
|---|---|---|---|---|---|---|---|---|---|---|---|
| | | | Cr $2p_{3/2}$ | | O 1s | Cr 2p | Ce $3d_{5/2}$ | Al 2p | Cl $2p_{3/2}$ | $Ce^{3+}/Ce^{4+}$ [b] | $Cr^{3+}/Cr^{6+}$ [b] |
| USY | – | 100.0 | – | – | – | – | – | – | – | – | – |
| $12.5CeO_2$-USY | – | – | – | – | 532.0 | – | 7.84 | 92.16 | – | 0.98 | – |
| $17.5Cr_2O_3$-USY | – | – | 577.4 | 579.8 | 531.8 | 17.90 | – | 82.10 | – | – | 2.62 |
| $17.5Cr_2O_3$-$12.5CeO_2$-USY | – | – | 578.6 | 580.6 | 531.8 | 42.75 | 10.20 | 47.05 | – | 1.24 | 1.69 |
| USY-A[a] | 11.4 | 90.1 | – | – | – | – | – | – | – | – | – |
| $12.5CeO_2$-USY-A | 1.1 | 84.1 | – | – | 532.1 | – | 12.58 | 85.21 | 2.21 | 0.74 | – |
| $17.5Cr_2O_3$-$12.5CeO_2$-USY-A | 0.6 | 86.6 | 576.6 | 578.2 | 531.8 | 38.45 | 10.23 | 47.03 | 4.29 | 1.31 | 2.00 |

[a] A: catalyst after 100 h test.
[b] Calculated from the peak area under the curves.

indicated by a lower BET surface area (Table 1), together with the increased dealumination and consequent loss of acidity caused by $Cr_2O_3$ impregnation over $Cr_2O_3$-$CeO_2$-USY catalysts [39]. With respect to the $R_{sw}$ (ratio of strong acidity concentration to weak acidity concentration) values of all the samples, we can see that the modified USY catalysts show different changes in $R_{sw}$ compared with that of USY zeolite. The $R_{sw}$ is much lower over $12.5CeO_2$-USY(1.20) than that of USY zeolite (1.74), indicating the addition of $CeO_2$ results in more obvious reduction of strong acidity. However, the $R_{sw}$ shows an evident increment over $17.5Cr_2O_3$-USY, demonstrating that the addition of $Cr_2O_3$ leads to less loss in weak acidity. For $Cr_2O_3$-$CeO_2$-USY catalysts, $11.5Cr_2O_3$-$12.5CeO_2$-USY and $23.5Cr_2O_3$-$12.5CeO_2$-USY exhibits more decrease in strong acidity while $17.5Cr_2O_3$-$12.5CeO_2$-USY shows a slight more loss in weak acid sites. Therefore, a relatively higher $R_{sw}$ value is observed over $17.5Cr_2O_3$-$12.5CeO_2$-USY, which may be associated with the stronger interaction between $Cr_2O_3$ and $CeO_2$ species over the catalyst. The $R_{sw}$ value of each catalyst decreases in the order of USY > $17.5Cr_2O_3$-$12.5CeO_2$-USY ≈ $17.5Cr_2O_3$-USY > $12.5CeO_2$-USY = $11.5Cr_2O_3$-$12.5CeO_2$-USY ≈ $23.5Cr_2O_3$-$12.5CeO_2$-USY.

### 3.1.3. Redox property

Fig. 3 shows the $H_2$-TPR profiles of $CeO_2$ and modified USY zeolite catalysts. For pure $CeO_2$, three reduction peaks are observed. The first two peaks below 600 °C are ascribed to the reduction of surface and sub-surface oxygen, and the third one above 600 °C is assigned to the reduction of bulk oxygen [31]. Due to the high dispersion of $CeO_2$ on the surface of USY zeolite, all the reduction peaks evidently shift to lower temperature range over $12.5CeO_2$-USY, and the $H_2$ consumption for $12.5CeO_2$-USY is also increased compared with that for pure $CeO_2$. The results indicate that the interaction between $CeO_2$ and USY zeolite improves the mobility of the oxygen species over the catalyst. Moreover, the broad peak observed within the temperature range of 300–600 °C also demonstrates the enhanced redox property of $12.5CeO_2$-USY [33]. Two reduction peaks are detected over $17.5Cr_2O_3$-USY as reported in the literature [40,41]. Peak δ is ascribed to reduction of highly dispersed $Cr_2O_3$ species, and peak ε is attributed to the reduction of $Cr_2O_3$ with large particle size. However, only one broadened reduction peak is observed at lower temperature range over $Cr_2O_3$-$CeO_2$-USY catalysts. As the $Cr_2O_3$ content increases, peak δ moves to higher temperature and the peak-temperature over $23.5Cr_2O_3$-$17.5CeO_2$-USY is similar to that over $17.5Cr_2O_3$-USY. It may be due to the aggregation of $Cr_2O_3$ particles over the catalyst where relatively high $Cr_2O_3$ content existing. At the same time, peak ε is gradually visible in $17.5Cr_2O_3$-$12.5CeO_2$-USY and $23.5Cr_2O_3$-$12.5CeO_2$-USY with lower peak-temperature and weaker peak intensity compared to that in $17.5Cr_2O_3$-USY. The results indicate that the interaction between $Cr_2O_3$ and $CeO_2$ species improves the mobility of oxygen species in the catalysts and enhances the reduction of both $Cr_2O_3$ species. Additionally, the intensity of the reduction peaks ascribed to the oxygen species in $CeO_2$ over $Cr_2O_3$-$CeO_2$-USY catalysts is evidently reduced compared with that over $12.5CeO_2$-USY. We suggest that the interaction between $Cr_2O_3$ and $CeO_2$ species also weakens the Ce—O bond and promotes the reduction of $CeO_2$. However, the $H_2$ consumption is affected little by the interaction between $Cr_2O_3$ and $CeO_2$ species as listed in Table 1.

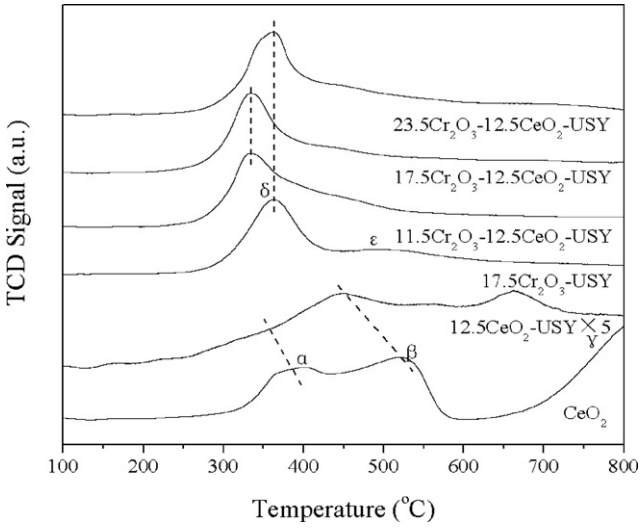


**Fig. 3.** $H_2$-TPR profiles of the catalysts.

## 3.2. Catalytic performance results

### 3.2.1. DCM decomposition

Fig. 4 presents the catalytic performance for DCM decomposition over USY zeolite and modified USY zeolite catalysts. As presented in Fig. 4(A), the catalytic activity for DCM destruction is higher over modified USY zeolite catalysts than that over USY zeolite, especially over $17.5Cr_2O_3$-$12.5CeO_2$-USY, suggesting that the interaction between $Cr_2O_3$ and $CeO_2$ species is beneficial for DCM destruction. The catalytic activity for DCM destruction over the catalysts based on $T_{90}$ (temperature when 90% conversion obtained) decreases in the order of $17.5Cr_2O_3$-$12.5CeO_2$-USY(281 °C) > $12.5CeO_2$-USY(340 °C) > USY(370 °C). As presented in Fig. 4(B), $CH_3Cl$ is the only by-product detected during DCM destruction. Large concentration of $CH_3Cl$ is detected over USY zeolite, which is much smaller over modified USY catalysts, especially over $17.5Cr_2O_3$-$12.5CeO_2$-USY. The results demonstrate that the addition of $Cr_2O_3$ together with the interaction between $Cr_2O_3$ and $CeO_2$ species inhibits the production of $CH_3Cl$. As shown in Fig. 4(C), large amount of CO is produced over USY during DCM decomposition, especially at higher temperature. However, the concentration of CO is decreased during the whole temperature range when $CeO_2$ and $Cr_2O_3$ are impregnated. The changing trend of CO is similar to that of $CH_3Cl$. That is better redox property the catalyst shows, less

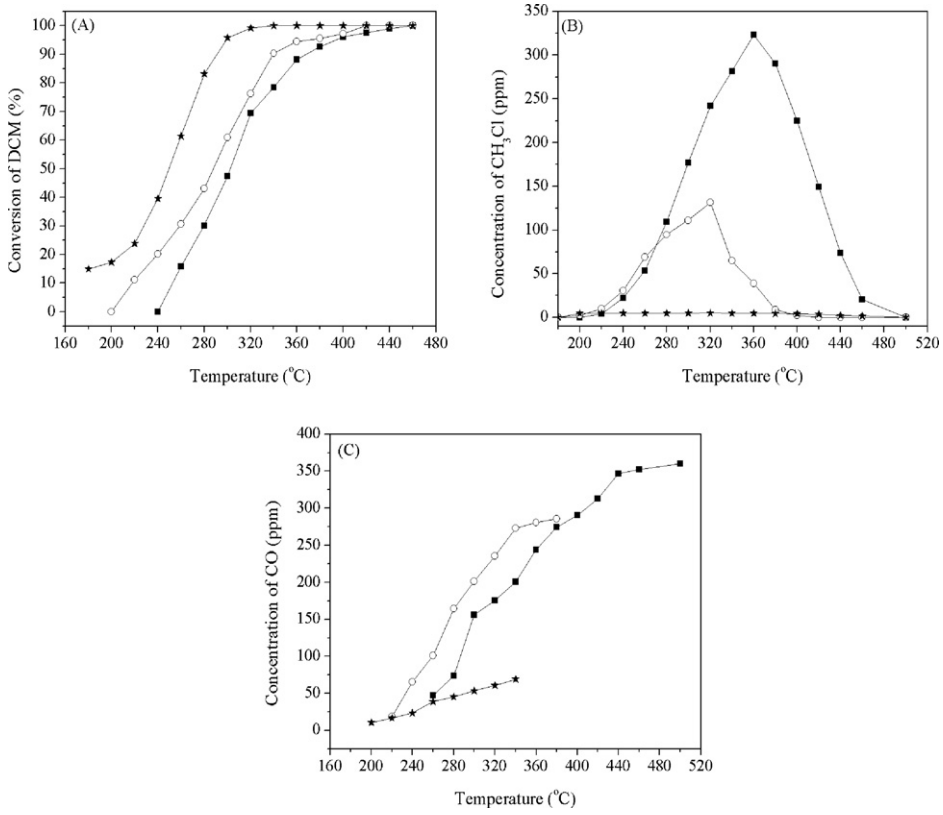


**Fig. 4.** The catalytic performance for DCM decomposition over the catalysts: (A) conversion of DCM; (B) concentration of $CH_3Cl$ and (C) concentration of CO (-■- USY, -○- 12.5$CeO_2$-USY, -★- 17.5$Cr_2O_3$-12.5$CeO_2$-USY).

CO forms. When DCM is completely decomposed, the selectivity to CO over each catalyst follows the order of 17.5$Cr_2O_3$-12.5$CeO_2$-USY (7%) ≪ 12.5$CeO_2$-USY(28.5%) > USY(36.7%).

Based on the research results in our group and the mechanism of DCM decomposition reported in previous literature [42], we suggest the mechanism of DCM decomposition over the catalysts is as follows. DCM first reacts with surface hydroxyl groups to generate adsorbed formaldehyde intermediates and HCl. Then, the formaldehyde disproportionates into methoxy and formate species. The former can react with HCl to form the by-product $CH_3Cl$, and the latter further converts to $CO_x$.

Combining with the physical–chemical characteristics of the catalysts, we suppose that the enhanced catalytic activity for DCM decomposition over 17.5$Cr_2O_3$-12.5$CeO_2$-USY is mainly due to the abundant acid sites and improved redox property, which are resulted from the strong interaction between $Cr_2O_3$ and $CeO_2$. With regard to the by-product $CH_3Cl$, it cannot be produced until a certain amount of adsorbed formaldehyde species are formed. In our research, over 12.5$CeO_2$-USY, DCM adsorption as well as HCl desorption is promoted ascribed to the abundant acid sites and the presence of plentiful OH groups. Moreover, the existence of weak Lewis acidity is beneficial to adsorption and accumulation of formaldehyde, promoting the formation of methoxy species. Therefore, large amount of $CH_3Cl$ resulted from the reaction between methoxy species and HCl is detected over 12.5$CeO_2$-USY. However, the further oxidation of formaldehyde and formate species is promoted over 17.5$Cr_2O_3$-12.5$CeO_2$-USY catalyst in the presence of $Cr_2O_3$ species especially $Cr^{6+}$ with stronger oxidation ability as well as more active oxygen species with better mobility resulted from the synergy between $Cr_2O_3$-$CeO_2$ and USY zeolite [43,44]. Therefore, small concentration of $CH_3Cl$ and CO is observed over 17.5$Cr_2O_3$-12.5$CeO_2$-USY.

In comparison with the previous study about CuO-$CeO_2$-USY catalyst for DCM destruction [45], we can see that at 300 °C, DCM conversion reaches as high as 95% over $Cr_2O_3$-$CeO_2$-USY, while that is only 80% over CuO-$CeO_2$-USY. The results indicate that $Cr_2O_3$-$CeO_2$-USY exhibits much better catalytic activity for DCM decomposition compared with CuO-$CeO_2$-USY.

### 3.2.2. TCE decomposition

Fig. 5 presents the catalytic performance for TCE decomposition over USY zeolite and modified USY zeolite catalysts. As shown in Fig. 5(A), TCE cannot be completely converted until the temperature is higher than 500 °C over USY zeolite. However, the catalytic activity for TCE destruction is obviously enhanced over modified USY zeolite catalysts, especially over 17.5$Cr_2O_3$-12.5$CeO_2$-USY, over which the temperature for TCE complete conversion is about 300 °C. On the basis of $T_{90,}$ the catalytic activity for TCE decomposition follows the order of 17.5$Cr_2O_3$-12.5$CeO_2$-USY(296 °C) > 12.5$CeO_2$-USY(422 °C) > USY(515 °C). As shown in Fig. 5(B), $C_2Cl_4$ is the only by-product observed during TCE decomposition. Small concentration of $C_2Cl_4$ with $T_{max}$ (temperature at which maximum concentration reaches) at higher temperature range is produced over USY zeolite. Large concentration of $C_2Cl_4$ is detected over 12.5$CeO_2$-USY with $T_{max}$ shifting to lower temperature range. The results indicate that the addition of $CeO_2$ resulting in the good redox property improves the decomposition of TCE to produce $C_2Cl_4$ at low temperature range and further oxidation of $C_2Cl_4$. Small concentration of $C_2Cl_4$ with $T_{max}$ observed at the lowest temperature is produced over 17.5$Cr_2O_3$-12.5$CeO_2$-USY, suggesting that the interaction between $Cr_2O_3$ and $CeO_2$, along with the synergy between $Cr_2O_3$-$CeO_2$ and USY zeolite results in more positive effect on the further oxidation of $C_2Cl_4$ at lower temperature range. As displayed in Fig. 5(C), large concentration

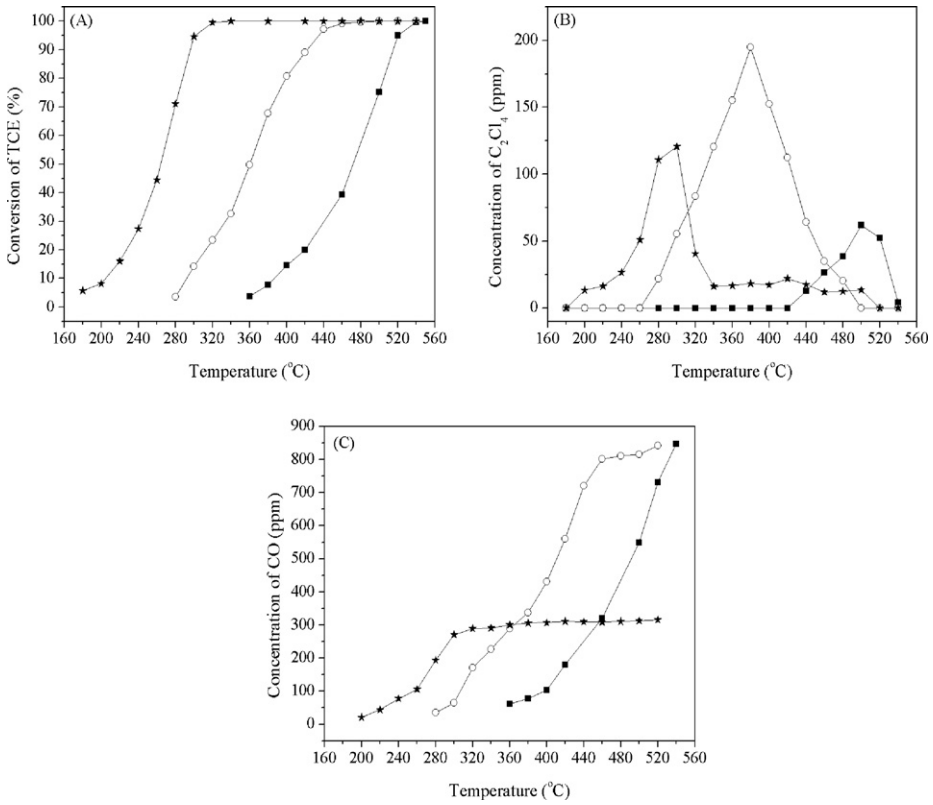


**Fig. 5.** The catalytic performance for TCE decomposition over the catalysts: (A) conversion of TCE; (B) concentration of $C_2Cl_4$ and (C) concentration of CO (-■- USY, -◯- 12.5$CeO_2$-USY, -★- 17.5$Cr_2O_3$-12.5$CeO_2$-USY).

of CO is detected over USY and 12.5$CeO_2$-USY, while much lower CO concentration is observed over 17.5$Cr_2O_3$-12.5$CeO_2$-USY. The selectivity to CO formation over the catalysts as TCE totally destructed decreases in the order of USY(42.3%) > 12.5$CeO_2$-USY(41.6%) > 17.5$Cr_2O_3$-12.5$CeO_2$-USY (31.6%).

It is known that the mechanism of TCE decomposition is as follows [46,47]. First, TCE reacts with OH groups over the surface of the catalyst via dehydrochlorination to form acyl chloride species, which can be further oxidized to $CO_x$ and $H_2O$ in the presence of active oxygen species. Meanwhile, the main by-product $C_2Cl_4$ is formed via the chlorination of TCE followed by dehydrochlorination in the presence of metal chloride or $Cl_2$ in the catalyst or reaction system. Combing with our research results, we speculate that the relatively higher value of $R_{sw}$ over 17.5$Cr_2O_3$-12.5$CeO_2$-USY(1.50) than that over 12.5$CeO_2$-USY(1.20) favors the dehydrochlorination of TCE. Moreover, the better redox property of the catalyst enhances the further oxidation of acyl chloride species. Therefore, 17.5$Cr_2O_3$-12.5$CeO_2$-USY exhibits the best catalytic activity for TCE decomposition. In the case of $C_2Cl_4$ production, $T_{max}$ value of $C_2Cl_4$ is much smaller over 17.5$Cr_2O_3$-12.5$CeO_2$-USY compared with that over 12.5$CeO_2$-USY. It may be attributed to the easier chlorination of chromium than that of cerium. Furthermore, the better redox property of the catalyst is beneficial to $Cl_2$ production via Deacon reaction ($2HCl + 1/2O_2 \leftrightarrow Cl_2 + H_2O$) over 17.5$Cr_2O_3$-12.5$CeO_2$-USY. Both of the above two factors are in favor of $C_2Cl_4$ production. Therefore, a certain amount of $C_2Cl_4$ is produced at low temperature range over 17.5$Cr_2O_3$-12.5$CeO_2$-USY. However, the large number of active oxygen species with better mobility and the presence of $Cr_2O_3$ species especially $Cr^{6+}$ with higher oxidizability [43,44] are beneficial to the rapid oxidation of $C_2Cl_4$ into $CO_x$ over the catalyst. Thus, only small amount of $C_2Cl_4$ is detected over 17.5$Cr_2O_3$-12.5$CeO_2$-USY. Moreover, due to the promoted $Cl_2$ production, the oxidation of carbon element to $CO_2$ is inhibited to some degree. Therefore, a certain amount of CO is produced during TCE decomposition.

Compared with the results obtained in our previous study on TCE catalytic decomposition over CuO-$CeO_2$-USY catalyst [45], we find that $Cr_2O_3$-$CeO_2$-USY shows a much higher TCE conversion than CuO-$CeO_2$-USY. $T_{90}$ is about 35 °C lower over $Cr_2O_3$-$CeO_2$-USY than that over CuO-$CeO_2$-USY. Moreover, the concentration of by-product $C_2Cl_4$ is evidently inhibited within the whole temperature range over $Cr_2O_3$-$CeO_2$-USY, while the production of $C_2Cl_4$ is obviously increased over CuO-$CeO_2$-USY.

### 3.2.3. DCE decomposition

Fig. 6 presents the catalytic performance for DCE decomposition over USY zeolite and modified USY zeolite catalysts. As presented in Fig. 6(A), 12.5$CeO_2$-USY exhibits the improved DCE conversion compared with USY. However, the further addition of $Cr_2O_3$ is detrimental to DCE conversion. It is due to the loss of acidity in the catalyst, which plays a critical role in the dehydrochlorination of DCE [39]. The catalytic activity for DCE conversion according to $T_{90}$ decreases in the following order: 12.5$CeO_2$-USY(246 °C) > 17.5$Cr_2O_3$-12.5$CeO_2$-USY(264 °C) > USY(310 °C). As presented in Fig. 6(B)–(E), there are only four by-products named $CH_3Cl$, $C_2H_3Cl$, $CH_3CHO$ and $CH_3COOH$ detected during DCE decomposition over the catalysts, without producing any high-chlorinated by-products. Moreover, the concentration of these by-products over 17.5$Cr_2O_3$-12.5$CeO_2$-USY is obviously smaller than that over the other two catalysts. Few concentration of $CH_3Cl$ produced over 17.5$Cr_2O_3$-12.5$CeO_2$-USY indicates that the addition of $Cr_2O_3$ significantly inhibits DCE cracking or promotes further oxidation of $CH_3Cl$. The concentration of $C_2H_3Cl$, $CH_3CHO$ and $CH_3COOH$ decreases obviously with $T_{max}$ evidently shifting to lower temperature, which demonstrates that the interaction between $Cr_2O_3$ and $CeO_2$ species improves

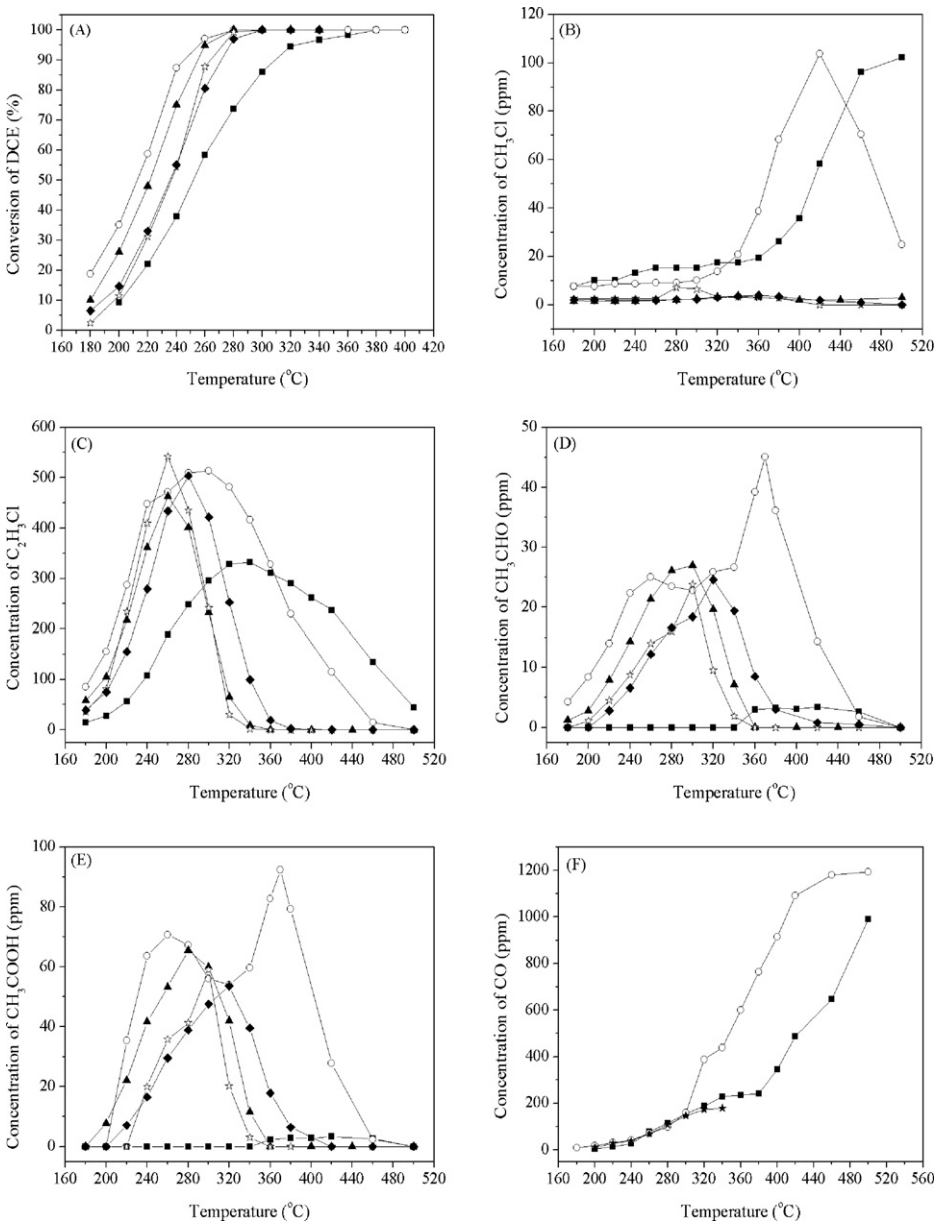


**Fig. 6.** The catalytic performance for DCE decomposition over the catalysts: (A) conversion of DCE; (B) concentration of $CH_3Cl$; (C) concentration of $C_2H_3Cl$; (D) concentration of $CH_3CHO$; (E) concentration of $CH_3COOH$ and (F) concentration of CO (-■- USY, -○- 12.5$CeO_2$-USY, -▲- 11.5$Cr_2O_3$-12.5$CeO_2$-USY, -☆- 17.5$Cr_2O_3$-12.5$CeO_2$-USY, -♦- 23.5$Cr_2O_3$-12.5$CeO_2$-USY).

the further dehydrochlorination and deeper oxidation of $C_2H_3Cl$. As presented in Fig. 6(F), large concentration of CO is produced over USY and 12.5$CeO_2$-USY. Especially, more CO is produced over 12.5$CeO_2$-USY than that over USY zeolite when the temperature is higher than 280 °C. However, only a small amount of CO is detected17.5$Cr_2O_3$-12.5$CeO_2$-USY. When DCE is completely decomposed, the selectivity to CO follows the order of 17.5$Cr_2O_3$-12.5$CeO_2$-USY(8.9%) ≪ USY(49.4%) < 12.5$CeO_2$-USY(56.6%).

On the basis of the above results, we deduce that 17.5$Cr_2O_3$-12.5$CeO_2$-USY exhibits the best catalytic performance for CVOCs decomposition due to the interaction between $Cr_2O_3$ and $CeO_2$, as well as the synergy between $Cr_2O_3$-$CeO_2$ and USY zeolite. In order to gain a further understanding about the influence of such interaction on the catalytic behavior for CVOCs decomposition, $Cr_2O_3$-$CeO_2$-USY catalysts with different $Cr_2O_3$ contents are prepared and evaluated for DCE decomposition.

The catalytic performance for DCE decomposition over $Cr_2O_3$-$CeO_2$-USY catalysts is also displayed in Fig. 6. The temperature when DCE can be completely converted rises with $Cr_2O_3$ content increasing over $Cr_2O_3$-$CeO_2$-USY catalysts (Fig. 6(A)). It can be due to the reduction of acidity concentration of the catalyst (listed in Table 1), which is a critical factor for DCE dehydrochlorination [39]. Trace amount of $CH_3Cl$ (always below 10 ppm) is detected over all the $Cr_2O_3$-$CeO_2$-USY catalysts (Fig. 6(B)). It can be ascribed to the $Cr_2O_3$ addition and the interaction between $Cr_2O_3$ and $CeO_2$ species, which inhibit DCE cracking or enhance the deeper oxidation of $CH_3Cl$. In comparison with 12.5$CeO_2$-USY, the amount of $C_2H_3Cl$, $CH_3CHO$ and $CH_3COOH$ shows an obvious reduction over $Cr_2O_3$-$CeO_2$-USY catalysts. As $Cr_2O_3$ content increases, the amount of those by-products does not show much difference, but $T_{max}$ of those by-products moves to higher temperature (Fig. 6(C)–(E)). Among all the catalysts, 17.5$Cr_2O_3$-12.5$CeO_2$-USY shows the best catalytic performance for DCE decomposition with relatively smaller $C_2H_3Cl$ production and the lowest $T_{max}$ of $C_2H_3Cl$. The results suggest that the relatively stronger interaction between $Cr_2O_3$ and $CeO_2$ as well as the synergy between $Cr_2O_3$-$CeO_2$ and

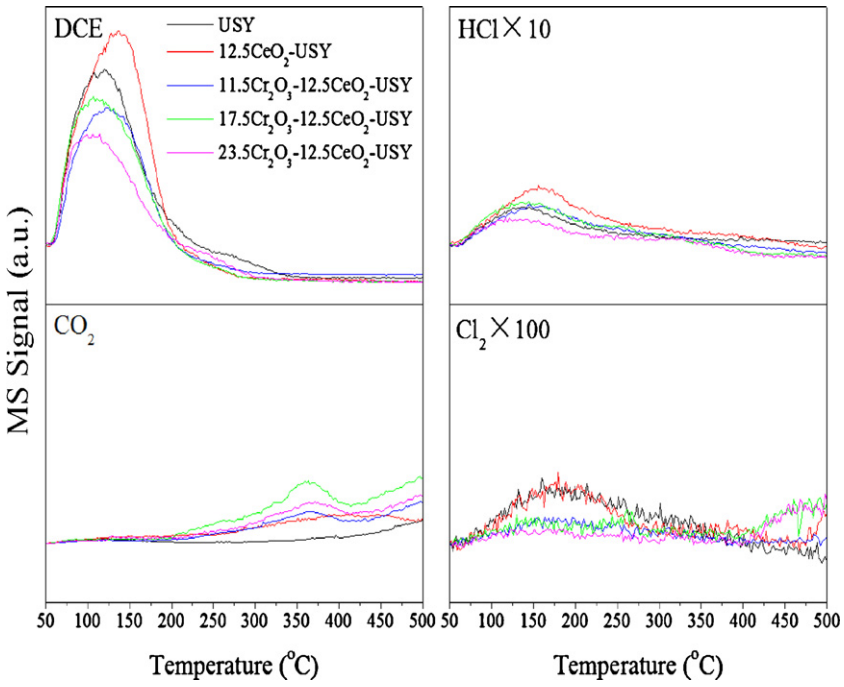


**Fig. 7.** TPSR profiles of DCE catalytic decomposition over the catalysts.

USY zeolite over $17.5Cr_2O_3$-$12.5CeO_2$-USY is appreciably in favor of further dehydrochlorination and deeper oxidation of $C_2H_3Cl$ and $CH_3Cl$.

In comparison with our previous study on the catalytic performance for DCE decomposition over CuO-$CeO_2$-USY catalyst [45], we find that not only the DCE conversion is higher over $Cr_2O_3$-$CeO_2$-USY, but also there is no high chlorinated by-products ($CHCl_3$ and $C_2Cl_4$) produced over $Cr_2O_3$-$CeO_2$-USY. Therefore, $Cr_2O_3$-$CeO_2$-USY catalyst shows much better catalytic performance for DCE decomposition than CuO-$CeO_2$-USY catalyst.

The adsorption–desorption behavior of DCE and the evolutions of the main products ($CO_2$, HCl and $Cl_2$) over USY zeolite and modified USY zeolite catalysts have been investigated by TPSR technique in order to evaluate adsorption capacity of the catalysts and the selectivity towards the formation of HCl and $CO_2$. As shown in Fig. 7, desorption accompanied with decomposition of DCE occurs at relatively low temperature range. The desorption peak of DCE is weakened with the peak-temperature shifting to lower temperature range as the Cr content increases over $Cr_2O_3$-$CeO_2$-USY catalysts compared with that over $12.5CeO_2$-USY. It can be due to the decrease in acidity in the catalysts leading to the weaker adsorption of DCE. The desorption peak is stronger over $17.5Cr_2O_3$-$12.5CeO_2$-USY than that over the other two $Cr_2O_3$-$CeO_2$-USY catalysts, indicating that the stronger interaction between $Cr_2O_3$ and $CeO_2$ over the catalyst enhances the adsorption of DCE. $CO_2$ can be detected at temperature as low as 200 °C over $12.5CeO_2$-USY and $Cr_2O_3$-$CeO_2$-USY catalysts, which cannot be detected until the temperature is higher than 350 °C over USY zeolite. Moreover, $CO_2$ production over $Cr_2O_3$-$CeO_2$-USY catalysts is obviously increased compared with that over $12.5CeO_2$-USY, suggesting that the interaction between $Cr_2O_3$ and $CeO_2$ shows an improvement in deeper oxidation of DCE and the selectivity to $CO_2$ formation. Especially for $17.5Cr_2O_3$-$12.5CeO_2$-USY, the largest amount of $CO_2$ is produced over the catalyst. Interestingly, one more peak is observed in the range of 320–400 °C over $Cr_2O_3$-$CeO_2$-USY catalysts. It may be ascribed to a combined signal of $CO_2$ production and desorption, which is adsorbed at low temperature on the catalysts [48]. The formation of $CO_2$ shows a good consistence with partial oxidation products ($CH_3CHO$, $CH_3COOH$ and CO) formation over the catalysts. That is $17.5Cr_2O_3$-$12.5CeO_2$-USY with best redox property and high oxidizability in the presence of $Cr^{6+}$ favors the formation of $CO_2$. Therefore, smallest CO concentration is detected among these catalysts. Relatively lower selectivity to CO over USY zeolite than that over $12.5CeO_2$-USY can be ascribed to the less production of $CH_3CHO$ and $CH_3COOH$ as well as sever coke deposit over USY, which will be discussed in the later part of our manuscript. In comparison with the evolutions of HCl and $Cl_2$, HCl is considered as the major chlorinated product within the temperature range 50–400 °C, which is a preferred chlorinated product instead of $Cl_2$. As the temperature further increases, $Cl_2$ production shows a slight increase over $12.5CeO_2$-USY and $Cr_2O_3$-$CeO_2$-USY catalysts. The results indicate that the oxidation of HCl to $Cl_2$ via the Deacon reaction is enhanced [42,49] due to the better deeper oxidation ability of the catalyst.

According to the reported literature [46,50], the mechanism of DCE decomposition over acid catalysts is known as follows. The decomposition occurs via dehydrochlorination of DCE into vinyl chloride in the presence of acid sites. This intermediate can be attacked by nucleophilic oxygen species from the catalyst to form chlorinated alkoxide species, which readily decompose to gradually generate acetaldehyde, acetates and $CO_x$. Combining with the results of DCE decomposition and characteristics of the catalysts, we deduce that assigned to the decrease in the concentration of acidity, especially the weak acidity (Lewis acidity) over $Cr_2O_3$-$CeO_2$-USY catalysts, which is the critical factor to the dehydrochlorination of DCE, the DCE conversion is lower over $Cr_2O_3$-$CeO_2$-USY catalysts than that over $12.5CeO_2$-USY with relatively more weak acid sites. However, the relatively high percentage of strong acidity over $Cr_2O_3$-$CeO_2$-USY catalysts promotes the further dehydrochlorination of $C_2H_3Cl$. Moreover, the deeper oxidation of $C_2H_3Cl$ and $CH_3Cl$ into $CO_2$ is enhanced over $Cr_2O_3$-$CeO_2$-USY catalysts, due to the presence of $Cr_2O_3$ with strong oxidation ability as well as more active oxygen species with better mobility resulted from the interaction between $Cr_2O_3$ and $CeO_2$ [25,26]. Especially for $17.5Cr_2O_3$-$12.5CeO_2$-USY, smaller concentration of main by-products and higher selectivity to $CO_2$ formation is observed assigned to the relatively higher percentage of strong acidity ($R_{sw}$ = 1.50) and better redox property.

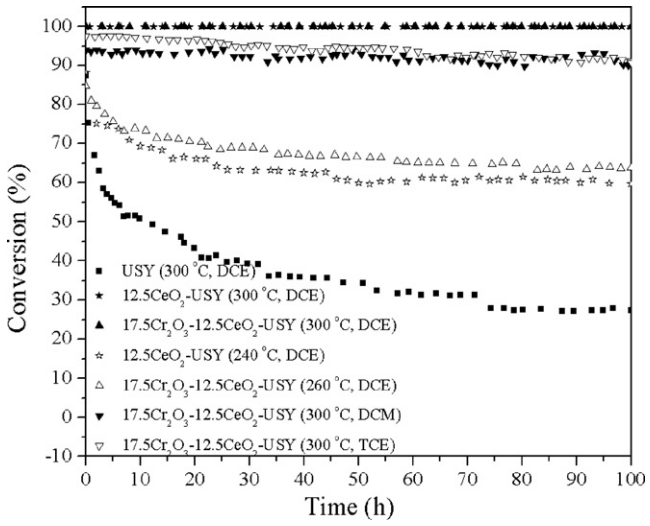


**Fig. 8.** The conversion of CVOCs catalytic decomposition over the catalysts as a function of time on stream.

### 3.3. Durability results

Based on the results above, USY, $12.5CeO_2$-USY and $17.5Cr_2O_3$-$12.5CeO_2$-USY are chosen to investigate the effect of interaction between $Cr_2O_3$ and $CeO_2$, as well as the synergy between $Cr_2O_3$-$CeO_2$ and USY zeolite on the durability of the catalysts. First, we evaluate the effect of the interaction between $Cr_2O_3$ and $CeO_2$ on the stability of these catalysts for DCE decomposition. As shown in Fig. 8, under the same given condition (300 °C, 15,000 $h^{-1}$), DCE conversion falls rapidly in the initial stage of the reaction and decreases from 87 to 27% over USY after 100 h tests, while the conversion maintains at 100% over modified USY zeolite catalysts. The results indicate that the modification evidently improves the durability of the catalyst. As is known, a certain part of the catalyst bed may not participate in the reaction when the conversion reaches 100%. Therefore, we re-evaluated the durability of these two fresh catalysts start with relatively low initial conversions. As shown in Fig. 8 DCE conversion decreases within the first 30 h, from 85 to 68% and 75 to 63% over $17.5Cr_2O_3$-$12.5CeO_2$-USY and $12.5CeO_2$-USY, respectively. Then, it changes little during the rest time of the long term test. After 100 h test, the conversion of DCE maintains at 64 and 60% over $17.5Cr_2O_3$-$12.5CeO_2$-USY and $12.5CeO_2$-USY, respectively. The results indicate that the modified catalysts also show deactivation to a certain extent during the long term reaction. However, the promotion to the durability of $17.5Cr_2O_3$-$12.5CeO_2$-USY is observed due to the modification especially the strong interaction between $Cr_2O_3$ and $CeO_2$ over the catalyst. Furthermore, we investigate the stability of $17.5Cr_2O_3$-$12.5CeO_2$-USY in the oxidation of DCM and TCE, in order to investigate the effect of reactant structure on the stability of the catalyst. We can see from Fig. 8 that the catalyst shows a stable conversion at about 91–92% for DCM destruction, and only a slight decrease in conversion (about 6%) is found for TCE decomposition. The results evidence again that $17.5Cr_2O_3$-$12.5CeO_2$-USY exhibits the good stability during CVOCs decomposition. Combining with the activity results, we can see that in comparison with DCE decomposition, the promotion on the conversion of DCM and TCE also brings in the better stability of the catalyst.

It is known that coke deposit is one of the factors to deactivation of zeolite catalysts [51]. As reported in Table 2, severe coke deposit is observed over USY, while much lower coke content is detected over $12.5CeO_2$-USY and $17.5Cr_2O_3$-$12.5CeO_2$-USY. It can be due to the presence of abundant oxygen species in the two catalysts, which favors the deeper oxidation of DCE into $CO_2$ and inhibits the coke production during the long term reaction. In particular, there is nearly no coke deposit occurs over $17.5Cr_2O_3$-$12.5CeO_2$-USY, indicating the coke deposit is evidently inhibited ascribed to the better mobility of oxygen species resulted from the strong interaction between $Cr_2O_3$ and $CeO_2$. The coke content over each catalyst increases following the order of $17.5Cr_2O_3$-$12.5CeO_2$-USY < $12.5CeO_2$-USY ≪ USY, which is the same as the order of the durability of the catalysts: $17.5Cr_2O_3$-$12.5CeO_2$-USY > $12.5CeO_2$-USY ≫ USY. Therefore, we suggest that the coke deposit is one of the factors to the deactivation of the catalysts. Furthermore, due to the strong interaction between $Cr_2O_3$ and $CeO_2$ that results in the better mobility of active oxygen species in the catalyst, the coke deposit is inhibited and the durability of the catalyst is improved.

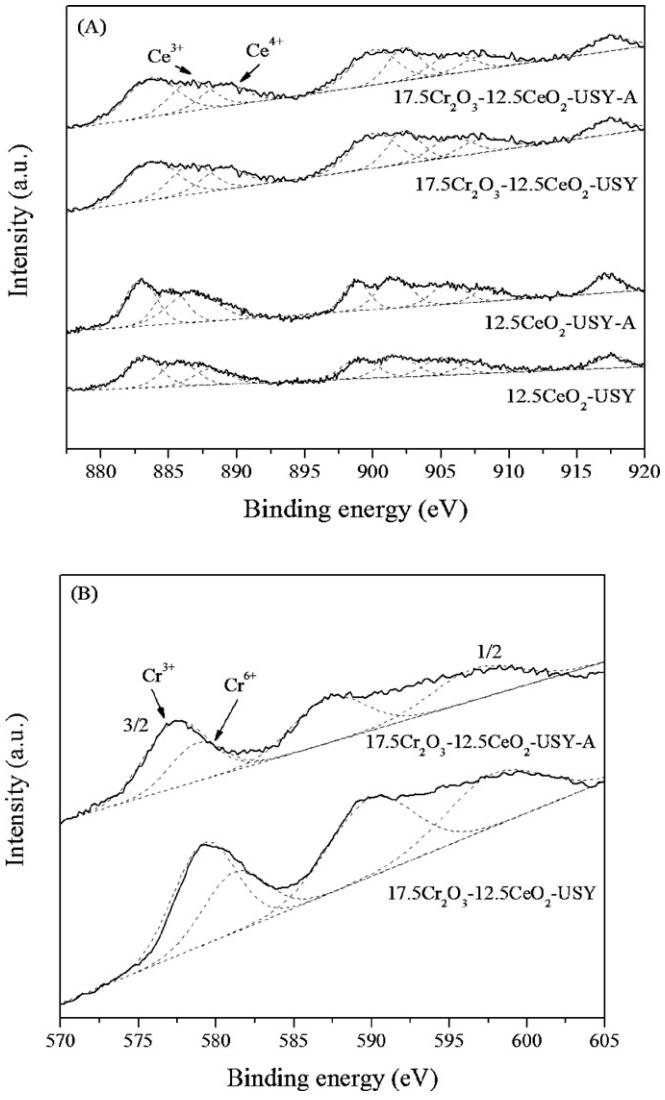


**Fig. 9.** XPS spectra of fresh and used catalysts: (A) Ce $3d_{5/2}$ and (B) Cr 2p ('A' stands for catalyst after 100 h tests).

It is reported in the literature that $CeO_2$ may be chlorinated by Cl species produced during CVOCs decomposition to form non-active phases, such as $CeOCl_2$ and $CeCl_3$ [52,53], which will result in the decrease in active components. Fig. 9 presents the XPS spectra of fresh and used catalysts. The binding energy and relative abundance of main elements are listed in Table 2. The binding energy of O 1s over $12.5CeO_2$-USY and $17.5Cr_2O_3$-$12.5CeO_2$-USY is about 531 eV, indicating the oxygen species in the catalysts are ascribed to oxygen vacancy or OH groups with good mobility [54].

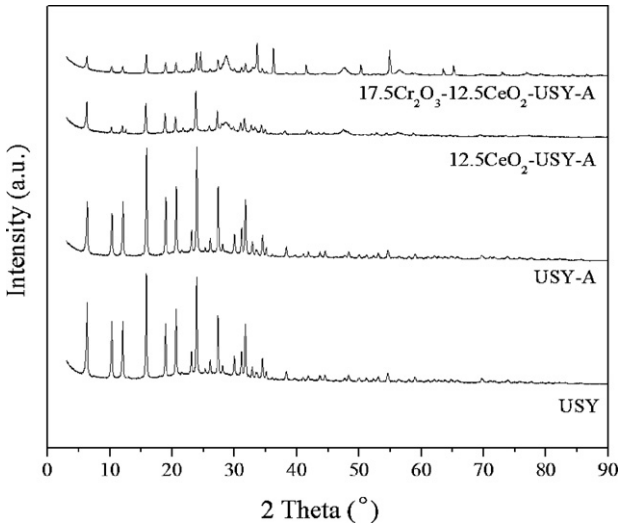


**Fig. 10.** XRD patterns of the catalysts after 100 h test ('A' stands for catalyst after 100 h tests).

After 100 h tests, the binding energy of O 1s changes little. As shown in Fig. 9(A) and Table 2, distinct spectra of $Ce^{3+}$ and $Ce^{4+}$ are observed over 12.5$CeO_2$-USY and 17.5$Cr_2O_3$-12.5$CeO_2$-USY catalysts [34,52,55,56], and the presence of $Ce^{3+}$ is associated with the formation of oxygen vacancy [34]. For 12.5$CeO_2$-USY catalyst, the ratio of $Ce^{3+}/Ce^{4+}$ is much lower over 12.5$CeO_2$-USY-A than that over 12.5$CeO_2$-USY, which indicates the decrease in oxygen vacancy after 100 h tests. A certain amount of Cl is also detected over 12.5$CeO_2$-USY-A. It is supposed that Cl species produced during DCE decomposition may adsorb on the surface blocking the active sites, or combined with $CeO_2$ to form non-active species $CeOCl_2$ and $CeCl_3$ adsorbing on the surface of the catalyst [33,52,53], which may lead to the deactivation of the catalyst. In the case of 17.5$Cr_2O_3$-12.5$CeO_2$-USY catalyst, the ratio of $Ce^{3+}/Ce^{4+}$ and the Al content changes little over 17.5$Cr_2O_3$-12.5$CeO_2$-USY-A compared with that over 17.5$Cr_2O_3$-12.5$CeO_2$-USY. It demonstrates that the strong interaction between $Cr_2O_3$ and $CeO_2$ improves the resistance to chlorination of $CeO_2$ and HCl attack on the framework of USY zeolite. As presented in Fig. 9(B) and Table 2, distinct spectra of $Cr^{3+}$ and $Cr^{6+}$ are visible over 17.5$Cr_2O_3$-12.5$CeO_2$-USY catalyst [40]. Cr content on the surface of the catalyst decreases to some extent after 100 h test. ICP-AES results also reveal that Cr element in the catalyst reduces by about 10%. It is supposed that $Cr_2O_3$ interacting weakly with $CeO_2$ may combine with Cl species in the form of volatile $CrO_2Cl_2$ [12], which will cause the loss of active components. It may be the factor to the deactivation of 17.5$Cr_2O_3$-12.5$CeO_2$-USY at the initial stage of the long term test.

We know that HCl produced during CVOCs oxidation will damage Al—O bond and cause the damage of zeolite framework [57,58]. Thus, the XRD analysis of the catalysts after 100 h tests is performed. As presented in Fig. 10, the catalysts after 100 h test maintain almost the same framework as fresh USY zeolite, and the crystallinity of the used catalysts is still higher than 80% as reported in Table 2. The results indicate that all the catalysts show high resistance to HCl attack. The higher crystallinity of 17.5$Cr_2O_3$-12.5$CeO_2$-USY-A as well as the less change of Al content suggests that the strong interaction between $Cr_2O_3$ and $CeO_2$ improves the structure stability of the catalyst. It is totally different from the results obtained in our previous study about the stability of CuO-$CeO_2$-USY catalysts during DCE decomposition, during the long term tests, the zeolite framework of CuO-$CeO_2$-USY completely changes [45].

## 4. Conclusions

The chromium and cerium modified catalysts were prepared by impregnation method and investigated in terms of catalytic decomposition of DCE, DCM and TCE. The results reveal that the $Cr_2O_3$ addition leads to the aggregation of $CeO_2$ particles on USY zeolite due to the easier entrance of $Cr^{3+}$ into pore channel of USY zeolite. The decrease in strong acid sites is affected more by $CeO_2$ addition, while the loss of weak acid sites is mainly influenced by $Cr_2O_3$ addition. There are two types of active sites in the catalysts. The acidic site is the active center for dehydrochlorination of CVOCs, and the metal oxide is the center providing active oxygen species for CVOCs deeper oxidation. The interaction between $Cr_2O_3$ and $CeO_2$ optimizes the concentration ratio of strong acidity to weak acidity and improves the mobility of oxygen species over $Cr_2O_3$-$CeO_2$-USY catalysts, which is beneficial to the dehydrochlorination of CVOCs and deeper oxidation of the intermediates, respectively. Therefore, $Cr_2O_3$-$CeO_2$-USY catalysts exhibit higher catalytic performance for the decomposition of DCE, DCM and TCE. In particular, 17.5$Cr_2O_3$-12.5$CeO_2$-USY with higher percentage of strong acidity, abundant active oxygen species with better mobility and the stronger synergy between $Cr_2O_3$-$CeO_2$ and USY zeolite, presents higher conversion of DCE, DCM and TCE, lower concentration of main by-products, higher selectivity to HCl and $CO_2$. In addition, the stronger interaction between $Cr_2O_3$ and $CeO_2$ species as well as the synergy between $Cr_2O_3$-$CeO_2$ and USY zeolite over 17.5$Cr_2O_3$-12.5$CeO_2$-USY enhances the stability of active components, and improves the resistant to coke deposit along with HCl attack on the catalyst. Therefore, 17.5$Cr_2O_3$-12.5$CeO_2$-USY shows better durability and structure stability during the long term exposure to DCE.

## Acknowledgments

We gratefully acknowledge the financial support from the Ministry of Science and Technology of China (no. 2011AA03A406) and Nature Science Foundation of China (no. 21177110).

## References

[1] E.C. Moretti, Practical Solutions for Reducing Volatile Organic Compounds and Hazardous Air Pollutants, Center for Waste Reduction Technologies of the American Institute of Chemical Engineers, New York, 2001.
[2] J.R. González-Velasco, A. Aranzabal, J.I. Gutiérrez-Ortiz, R. López-Fonseca, M.A. Gutiérrez-Oritiz, Appl. Catal. B 19 (1998) 189–197.
[3] P. Hunter, S.T. Oyama, Control of Volatile Organic Compounds Emissions: Conventional and Emerging Technologies, Wiley-Interscience, New York, 2000.
[4] S. Pitkäaho, S. Ojala, T. Maunula, A. Savimäki, T. Kinnunen, R.L. Keiski, Appl. Catal. B 102 (2011) 395–403.
[5] X.Y. Wang, Q. Kang, D. Li, Appl. Catal. B 86 (2009) 166–175.
[6] B. de Rivas, R. López-Fonseca, C. Sampedro, J.I. Gutiérrez-Ortiz, Appl. Catal. B 90 (2009) 545–555.
[7] B. de Rivas, R. López-Fonseca, M.Á. Gutiérrez-Ortiz, J.I. Gutiérrez-Ortiz, Appl. Catal. B 101 (2011) 317–325.
[8] E. Finocchio, G. Sapienza, M. Baldi, G. Busca, Appl. Catal. B 51 (2004) 143–148.
[9] J.A. González-Marcos, J.R. González-Velasco, Catal Today, doi:10.1016/j.cattod.2010.11.065.
[10] M. Kułażyński, J.G. van Ommen, J. Trawczyński, J. Walendziewski, Appl. Catal. B 36 (2002) 239–247.
[11] T.F. Garetto, C.I. Vignatti, A. Borgna, A. Monzón, Appl. Catal. B 87 (2009) 211–219.
[12] C.H. Cho, S.K. Ihm, Environ. Sci. Technol. 36 (2002) 1600–1606.
[13] K. Everaert, J. Baeyens, J. Hazard. Mater. 109B (2004) 113–139.
[14] G. Sinquin, C. Petit, S. Libs, J.P. Hindermann, A. Kiennemann, Appl. Catal. B 27 (2001) 105–115.
[15] A.M. Padilla, J. Corella, J.M. Toledo, Appl. Catal. B 22 (1999) 107–121.
[16] D.-C. Kim, S.K. Ihm, Environ. Sci. Technol. 35 (2001) 222–226.
[17] T. Tanilimiş, S. Atalay, H.E. Alpay, F.S. Atalay, J. Hazard. Mater. B90 (2002) 157–167.
[18] H. Rotter, M.V. Landau, M. Herskowitz, Environ. Sci. Technol. 39 (2005) 6845–6850.
[19] B. Miranda, E. Díaz, S. Ordóñez, A. Vega, F.V. Díez, Chemosphere 66 (2007) 1706–1715.
[20] S. Krishnamoorthy, J.A. Rivas, M.D. Amiridis, J. Catal. 193 (2000) 264–272.

[21] S.D. Yim, K-H. Chang, D.J. Koh, I-S. Nam, Y.G. Kim, Catal. Today 63 (2000) 215–222.
[22] S.D. Yim, I-S. Nam, J. Catal. 221 (2004) 601–611.
[23] F. Bertinchamps, C. Grégoire, E.M. Gaigneaux, Appl. Catal. B 66 (2006) 1–9.
[24] M. Kang, M.W. Song, C.H. Lee, React. Kinet. Catal. Lett. 80 (2003) 131–138.
[25] M. Kang, C.-H. Lee, Appl. Catal. A 266 (2004) 163–172.
[26] L.C.A. Oliveira, R.M. Lago, J.D. Fabris, K. Sapag, Appl. Clay Sci. 39 (2008) 218–222.
[27] G.A. Atwood, H.L. Greene, P. Chintawar, R. Rahcapudi, B. Ramachandran, C.A. Vogel, Appl. Catal. B 18 (1998) 51–61.
[28] S. Kawi, M. Te, Catal. Today 44 (1998) 101–109.
[29] S.K. Agarwal, J.J. Spivey, J.B. Butt, Appl. Catal. A 82 (1992) 259–275.
[30] R. Rachapudi, P.S. Chintawar, H.L. Greene, J. Catal. 185 (1999) 58–72.
[31] J.M. Zhou, L.M Zhao, Q.Q. Huang, R.X. Zhou, X.K. Li, Catal. Lett. 127 (2009) 277–284.
[32] Q.Q. Huang, X.M. Xue, R.X. Zhou, J. Hazard. Mater. 183 (2010) 694–700.
[33] Q.Q. Huang, X.M. Xue, R.X. Zhou, J. Mol. Catal. A 331 (2010) 130–136.
[34] J. Fan, X.D. Wu, X.D. Wu, Q. Liang, R. Ran, D. Weng, Appl. Catal. B 81 (2008) 38–48.
[35] L. Storaro, R. Ganzerla, M. Lenarda, R. Zanoni, A.J. López, P. l Olivera-Pastor, E.R. Castellón, J. Mol. Catal. A 115 (1997) 329–338.
[36] A. de Lucas, P. Cañizares, A. Durán, Appl. Catal. A 206 (2001) 87–93.
[37] R.L. Fonseca, S. Cibrián, J.I.G. Oritiz, M.A.G. Oritiz, J.R.G. Velasco, AIChE J. 49 (2003) 496–504.
[38] A.Z. Abdullah, M.Z.A. Bakar, S. Bhatia, J. Hazard. Mater. 129 (2006) 39–49.
[39] S. Chatterjee, H.L. Greene, Appl. Catal. A 98 (1993) 139–158.
[40] J. Słoczyński, J. Janas, T. Machej, J. Rynkowski, Appl. Catal. B 24 (2000) 45–60.
[41] C.M. Pradier, F. Rodrigues, P. Marcus, M.V. Landau, M.L. Kaliya, A. Gutman, M. Herskowitz, Appl. Catal. B 27 (2000) 73–85.
[42] B. Ramachandran, H.L. Greene, S. Chatterjee, Appl. Catal. B 8 (1996) 157–182.
[43] S. Chatterjee, H.L. Greene, Y.J. Park, J. Catal. 138 (1992) 179–194.
[44] S. Chatterjee, H.L. Greene, J. Catal. 130 (1991) 76–85.
[45] Q.Q. Huang, X.M. Xue, R.X. Zhou, J. Mol. Catal. A 344 (2011) 74–82.
[46] M.M.R. Feijen-Jeurissen, J.J. Jorna, B.E. Nieuwenhuys, G. Sinquin, C. Petit, J.-P. Hindermann, Catal. Today 54 (1999) 65–79.
[47] J.I. Gutiérrez-Ortiz, B. de Rivas, R. López-Fonseca, J.R. González-Velasco, Appl. Catal. A 269 (2004) 147–155.
[48] Z.X. Yang, B.L. He, Z.S. Lu, K. Hermansson, J. Phys. Chem. C 114 (2010) 4486–4494.
[49] J. Janas, R. Janik, T. Machej, E.M. Serwicka, E. Bielańska, Catal. Today 59 (2002) 241–248.
[50] B. de Rivas, R. López-Fonseca, J.R. González-Velasco, J.I. Gutíerrez-Ortiz, J. Mol. Catal. A 278 (2007) 181–188.
[51] A. Aranzabal, J.A. González-Marcos, M. Romero-Sáez, J.R. González-Velasco, M. Guillemot, P. Magnoux, Appl. Catal. B 88 (2009) 533–541.
[52] Q.G. Dai, X.Y. Wang, G.Z. Lu, Catal. Commun. 8 (2007) 1645–1649.
[53] Q.G. Dai, X.Y. Wang, G.Z. Lu, Appl. Catal. B 81 (2008) 192–202.
[54] G. Praline, B.E. Koel, R.L. Hance, H.-I. Lee, J.M. White, J. Electron Spectrosc. Relat. Phenom. 21 (1) (1980) 17–30.
[55] I. Atribak, A.B. López, A.G. Carcía, J. Mol. Catal. A 300 (2009) 103–110.
[56] P. Singh, M.S. Hegde, Chem. Mater. 21 (2009) 3337–3345.
[57] S. Karmakar, H.L. Greene, J. Catal. 138 (1992) 364–376.
[58] G.M. Bickle, T. Suzuki, Y. Mitarai, Appl. Catal. B 4 (1994) 141–153.